

## TEMPERATURE AND HEAVY ELEMENT ABUNDANCE PROFILES OF COOL CLUSTERS OF GALAXIES FROM ASCA

A. FINOGUENOV<sup>1,3</sup>, M. ARNAUD<sup>2</sup> AND L.P. DAVID<sup>3</sup><sup>1</sup> Max-Planck-Institut für extraterrestrische Physik, Giessenbachstraße, 85748 Garching, Germany<sup>2</sup> Service d'Astrophysique, CEA Saclay, 91191 Gif sur Yvette Cedex, France<sup>3</sup> Smithsonian Astrophysical Observatory, 60 Garden st., MS 2, Cambridge, MA 02138, USA

## ABSTRACT

We perform a spatially resolved X-ray spectroscopic study of a set of 18 relaxed clusters of galaxies with gas temperatures below 4 keV. Spectral analysis was done using ASCA/SIS data coupled with the spatial information contained in ROSAT/PSPC and Einstein/IPC observations. We derive the temperature profiles using single-temperature fits and also correct for the presence of cold gas at the cluster centers. For all of the clusters in the sample, we derive Si and Fe abundance profiles. For a few of the clusters, we also derive Ne and S abundance profiles. We present a comparison of the elemental abundances derived at similar overdensities as well as element mass-to-light ratios. We conclude that the preferential accretion of low entropy, low abundance gas into the potentials of groups and cold clusters can explain most of the observed trends in metallicity. In addition, we discuss the importance of energy input from SNe II on cluster scaling relations and on the relation between the observed scatter in the retainment of SN Ia products with differences between the epoch of cluster formation.

*Subject headings:* Abundances — galaxies: clusters: general — galaxies: evolution — intergalactic medium — stars: supernovae — X-rays: galaxies

## 1. INTRODUCTION

The intracluster medium (ICM) has long been a subject of research for analyzing elements produced and lost by galaxies. By determining the total mass in metals produced by the stellar population of a cluster, one can place constraints on the population of massive stars, or equivalently, the Initial Mass Function (IMF), and the integrated Type Ia supernovae (SNe Ia) rate. In addition, the abundance and distribution of heavy elements in the ICM are sensitive to the processes of hierarchical clustering and therefore provide a unique tool for accessing the details of how present-day clusters evolve.

In Finoguenov, David & Ponman (2000, hereafter FDP), we presented an extensive study of the distribution of heavy elements in groups and clusters and discussed the implications regarding the chemical enrichment of the intracluster medium. For clusters with the best photon statistics, we found that the Fe abundance decreases significantly with radius, while the Si abundance is either flat or decreases slightly. This results in an increasing Si/Fe ratio with radius and implies a radially increasing predominance of Type II SNe enrichment in clusters. In rich clusters, the overall Fe mass from SN II requires  $N_{SNII}/N_{SNIa} \sim 20$  within  $0.2r_{180}$  ( $r_{180}$  is the radius at which the mean cluster density is 180 times the critical density), substantially different from the balance in our Galaxy (7 : 1). SN Ia products show a strong central concentration in most clusters, suggesting a release mechanism with a strong density dependence (e.g., ram pressure stripping of infalling gas rich galaxies). Moreover, the Iron Mass-to-Light Ratio (IMLR) for SN Ia decreases with radius in most clusters. The dependence of [Si/Fe] vs [Fe/H] reveals a smaller role of SN II in the enrichment of groups compared to clusters, suggesting that SN II products were only weakly captured by the shallower potential wells of groups due to the possible high entropy of preheated gas.

In this *Paper*, we extend the approach developed in FDP to

systems with properties intermediate between cool groups and hot clusters. Given the temperature range of these systems, the ASCA/SIS sensitivity is sufficient to constrain the temperature distribution and determine the radial profiles of Fe and Si. For clusters with good photon statistics we can also constrain the distribution of Ne and S. We present new spectroscopic results for A262, A2197 (subclusters E and W), A539, MKW3S, MKW4S, MKW9, AWM4, HCG94, A779, A400, A2052, A2634, A4038 (Klemola 44), 2A0335+096, A2063, and A194. We also include an analysis of the Centaurus cluster to compare with the method of Ikebe et al. (1999).

This paper is organized as follows: in Sec. 2 we describe our analysis technique; temperature profiles are discussed in 3; in 4 we present the radial abundance profiles of Fe, Si, Ne and S; in 5 we analyze the elemental abundances derived at similar overdensities and their corresponding mass-to-light ratios with a further discussion of the roles of SN II in 5.1 & 5.2 and SN Ia in 5.3. Our main results are summarized in 6. We assume  $H_0 = 50 \text{ km s}^{-1} \text{ Mpc}^{-1}$ ,  $q = 0.5$  throughout the paper.

## 2. DATA REDUCTION

A detailed description of the ASCA observatory as well as the SIS detectors can be found in Tanaka, Inoue & Holt (1994) and Burke et al. (1991). All observations are screened using FTOOLS version 4.2 with standard screening criteria. The effect of the broad ASCA PSF is treated as described in Finoguenov et al. (1999) including the geometrical projection of the three-dimensional distribution of X-ray emitting gas. Our minimization routines are based on the  $\chi^2$  criterion. No energy binning is done, but a special error calculation is introduced as in Churazov et al. (1996) to properly account for small number statistics. Model fits to ROSAT (Truemper 1983) surface brightness profiles are used as input to the ASCA data modeling. The details of our minimization procedure for ASCA spectral analysis are described in Finoguenov and Ponman (1999). We adapted the XSPEC analysis package to perform the ac-

TABLE 1  
X-RAY AND OPTICAL QUANTITIES OF THE SAMPLE

Name	D Mpc	' kpc	$L_B$ $10^{11} L_\odot$	$R_{mes}$ Mpc	$L_{B,CD}$ $10^{11} L_\odot$	$R_c$ Mpc	$\alpha$	$\beta$	$r_c$ kpc	$\nwarrow$	$kT_{unc}$ keV	$\delta kT_{unc}$ keV	$kT_e$ keV	$\delta kT_e$ keV	$R_v$ Mpc
A2197E	177	49	4.25 <sup>1</sup>	0.29	2.7	0.38	0.89	0.35	17		1.097	0.07	1.097	0.07	1.291
A400	145	40	21. <sup>2</sup>	3.	0.81	0.08	0.83	0.56	180	SE W	1.83	0.16	1.83	0.16	1.67
A194	107	30	5.1 <sup>3</sup>	0.8	0.00	0.267	0.925	0.60	26	NE SW	2.12	0.43	2.12	0.43	1.79
A262	97	27	10. <sup>4</sup>	0.82	0.55	0.02	0.59	0.46	58	SE $\Rightarrow$ W	2.18	0.21	2.26	0.23	1.85
MKW4S	171	47	6.3 <sup>†</sup>	0.5	2.62	0.25	1.	0.51	124	SE	2.13	0.64	2.29	0.26	1.87
A539	174	48	38. <sup>5</sup>	2.	0.79	0.04	0.78	0.69	250	E	2.81	0.34	2.81	0.34	2.07
AWM4	195	57	6.4 <sup>†</sup>	0.5	1.09	0.25	1.	0.62	110		2.92	0.39	2.92	0.39	2.11
MKW9	240	65	6.7 <sup>†</sup>	0.5	1.46	0.25	1.	0.52	54	E W	2.66	0.57	2.92	0.43	2.11
A2197	183	50	3.0 <sup>1</sup>	0.31	1.90	0.185	0.94	0.43	53		2.21	0.49	3.05	0.82	2.15
A2634	189	52	70. <sup>6</sup>	1.5	1.57	0.324	0.47	0.69	448	SW	3.06	0.35	3.06	0.35	2.16
A4038	171	47	15. <sup>7</sup>	1.2	1.04	0.043	0.86	0.61	160	NW $\Rightarrow$ E	3.31	0.25	3.31	0.25	2.24
2A0335	211	57	7.3 <sup>†</sup>	0.5	0.71	0.25	1.	0.65	80		3.07	0.27	3.40	0.39	2.27
HCG94	253	68	7.0 <sup>†</sup>	0.5	0.29	0.25	1.	0.48	75	NE SE	2.94	0.45	3.45	0.50	2.29
A2052	210	57	26. <sup>6</sup>	1.5	1.10	0.139	0.7	0.64	100		3.24	0.32	3.46	0.39	2.29
A779	136	38	13.1 <sup>8</sup>	2.9	2.11	0.525	0.95	0.34	54	N S	2.97	0.39	3.56	0.53	2.33
MKW3S	273	73	9.4 <sup>†</sup>	0.5	1.67	0.25	1.	0.71	300	SE $\Rightarrow$ NW	3.45	0.47	3.79	0.53	2.40
CEN	63	18	48. <sup>9</sup>	1.0	1.40	0.230	0.88	0.44	28	N	3.56	0.28	3.82	0.29	2.41
A2063	214	58	12. <sup>6</sup>	0.5	1.91	0.253	0.94	0.69	220	N $\Rightarrow$ E	3.83	0.39	3.86	0.24	2.42

<sup>†</sup> Interpolated value using Eq.1 from FDP.

<sup>4</sup> Sakai et al. 1994

<sup>5</sup> Ostriker et al. 1988

<sup>6</sup> Cirimele et al. 1998

<sup>1</sup> present work

<sup>2</sup> Arnaud et al. 1992

<sup>3</sup> Nikogossyan et al. 1999

& Tammann 1997

<sup>7</sup> Green et al. 1990

<sup>8</sup> Trèvese et al. 1996

<sup>9</sup> Jerjen

tual fitting and error estimation. The spatially resolved spectral characteristics are quoted as the best fit solution plus an estimate of the 90 % confidence area of possible parameter variation based on the regularization technique (Press et al. 1992; Finoguenov and Ponman 1999). To study the systematic errors related to the spatially resolved spectroscopic analysis of the ASCA data, we follow the approach described in FDP. For all ROSAT imaging analysis we use the software described in Snowden et al. (1994) and references therein.

We use the MEKAL plasma code (Mewe et al. 1985, Mewe and Kaastra 1995, Liedahl et al. 1995) in all of our spectral analysis. All abundances are given relative to the solar values in Anders & Grevesse (1989). The abundances of He and C are fixed to their solar value. The remaining elements are combined into five groups for fitting: Ne; Mg; Si; S and Ar; and Ca, Fe, and Ni. We restrict our analysis to the energy range 0.8–7.0 keV to avoid the large systematic uncertainties at low energies, which prevent us from determining the O abundance. We do not report the Mg abundance due to the proximity of the Mg K lines with the poorly understood 4-2 transition lines of iron, which are strongest at temperatures of 2 to 4 keV (see Fabian et al. 1994 and Mushotzky et al. 1996).

Table 1 contains the optical and X-ray properties of our sample. Column (1) identifies the system, (2) adopted luminosity distance, (3) corresponding scale length, (4) total blue light along with a reference, (5) corresponding radius of the optical measurement, (6) B luminosity of the cD galaxy from NED, (7) core radius of the galaxy distribution, and (8) the slope  $\alpha$  of the modified King profile  $(1 + (r/R_c)^2)^{-3\alpha/2}$ . Columns (9–10) give the results of the cluster surface brightness fitting outside the central region using a  $\beta$  model. Since the outer region chosen for the spatial analysis only corresponds to a part of the cluster, due to e.g. number of CCDs read-out, in col. (11) we denote the position of the observed region relative to the cluster center with NW $\Rightarrow$ E denoting an area extending from the North-West to the East in a counterclockwise direction. Column (12)

gives the best fit cluster emission-weighted temperature, (13) the corresponding 90% error, (14) the best fit cluster emission-weighted hotter temperature in a two-temperature fit (data for the colder component are listed in Tab.2), (15) the corresponding 90% error, and (16) an estimate of the virial radius of the system ( $r_{180} = 1.23 T_{keV}^{0.5} h_{50}^{-1}$  Mpc; Evrard et al. 1996) using  $kT_e$ . Estimates of the virial radii using X-ray observations carried out in Finoguenov, Reiprich and Boehringer (2001) show that the actual virial radii are 20% lower than Evrard's value.

## 2.1. Optical data reduction

A modified King profile was assumed for the galaxy distribution. The core radius and slope were taken from the literature when available (the references are given in Table 1), otherwise we assumed average values of  $R_c = 0.25$  Mpc and  $\alpha = 1$ . For A779, A2197(E,W) and Centaurus, we fitted the cumulative galaxy distribution derived from the galaxy catalog of Trèvese et al (1997), Dixon, Godwin & Peach (1989) and Jerjen & Dressler (1997), respectively. Only galaxies brighter than the catalog completeness limit were considered. The corresponding background counts were estimated as described in Trèvese, Cirimele & Appodia (1996) for A779 and from the deep counts of the ESO-Sculptor Redshift Survey (Arnouts et al. 1997) for A2197. They are negligible in the later case. No background correction was applied for Centaurus; cluster members and background objects are distinguished in the catalog based on morphological criteria and we only considered definite cluster members. A2197 is a double cluster, as revealed by the X-ray morphology; one subcluster is centered on NGC 6160 (A2197W) and the other on NGC 6173 (A2197E). To limit confusion between the two components, we only considered the central region of each subcluster within 6' ( $\sim 300$  kpc) from its central galaxy. The galaxy distribution parameters of A4038 were derived from a fit to the surface density of galaxies published in Green, Godwin & Peach (1990, Table 4). The total blue light of each cluster within a given projected

radius is listed in Table 1. Some processing was required to obtain a set of homogeneous values from the published data (see the references in Table 1). The published luminosities of A194 and A262 were corrected for the faint end of the luminosity function (LF). We used a Schechter luminosity function with  $M_B^* = -20.6$  and  $\alpha = -1.25$  and converted the published limiting magnitudes to limiting luminosities taking into account interstellar absorption. The z-correction is negligible in our redshift range. The luminosities of A2052, A2063 and A2634 within 1.5 Mpc were computed using a Schechter LF and a modified King galaxy distribution with the parameters published in Cirimele et al (1997, 1998). The luminosity of A779 within 2.85 Mpc was computed from the luminosity function determined by Trèvese, Cirimele & Appodia (1996) in that region. The normalization of the LF was deduced from the published galaxy counts within the completeness limit. For these four clusters and A400 the luminosity in the V-band was converted into a B-band luminosity assuming  $L_V = 1.3L_B$ . The luminosity of the Centaurus cluster was estimated using the catalog of Jerjen & Dressler (1997). We summed the luminosities of all possible cluster members within 1.5 Mpc from the cluster center and down to the catalog completeness limit ( $M_B = -15.3$ ). The error induced by the uncertainty on cluster membership is small. The luminosity is only 20% less if only definitive cluster members are considered. The correction for the faint end of the LF, estimated from the Schechter LF given in Jerjen & Tammann (1997), was found negligible. A similar procedure was performed for A2197W and A2197E using the galaxy catalog of Dixon, Godwin & Peach (1989), down to its completeness limit. The background correction, estimated statistically from the deep counts in each magnitude bin (Arnouts et al. 1997), is negligible (at the few % level) as well as the correction for incompleteness.

## 2.2. Details of X-ray data reduction

Although the analysis technique was intended to be similar for all of the clusters, some corrections were individually made, which we describe in this section.

A194, A2063, AWM4, and A539 have bright point-like sources in the field of view. In these cases we extract the spectra of point sources with both ROSAT/PSPC and ASCA/SIS, subtract the cluster background, analyze the spectra and then based on the ASCA response matrix estimate the contribution from these point sources to the regions selected for analysis of the diffuse cluster emission. For A194 the contribution of the point sources was severe at the center and we omit the central region of A194 from further discussion.

The 1996 observation of A400 was performed in 4-CCD mode which has significant SIS1 calibration problems, so we omit the SIS1 data from further analysis.

The observation of MKW9 has a high background, which is noticeable at the edges of the detector (due to warm CCDs as pointed out by Buote 2000). This background dominates the spectrum below 1 keV. We analyze and subtract the excess background and only fit the source spectrum in the 0.9–3.5 keV energy band. Thus, the Fe abundance for this cluster is derived from the L-shell line complex. Buote (2000) claims that the derived Fe abundance in MKW9 increases from 0.4 to 0.7 solar, when adding a second temperature component. We find that this conclusion depends on whether the high-energy part of the spectrum is included in the spectral fitting, and does not depend on the inclusion of the second temperature component as advocated by Buote (2000). While we attribute this effect

to uncertainties in the subtraction of the background, our error bars allow for both Fe abundance values. The spatial modeling of MKW9 was taken from an Einstein/IPC observation.

The spectral analysis of the MKW4S data reveals significant residuals at high energies which we attribute to an enhanced SIS background. Since the spectral data on this cluster are of poor quality at energies above 4 keV, this effect leads to a spurious rise in the derived temperature accompanied by an unacceptable large  $\chi^2$ . To overcome these difficulties, we restricted the spectral analysis to the 0.7–3.5 keV band. Thus, the Fe abundance for this cluster is derived from measurements of the L-shell line complex only.

For several clusters (MKW4S, AWM4, MKW9, A4038, HCG94, and MKW3S), whose observations have obvious calibration problems, we add a 10% systematic error at the 68% confidence level below 1.5 keV to the spectra. After the corrections mentioned in this section we are able to reduce the  $\chi^2$  values of the fit to acceptable values. A spatially resolved spectroscopic analysis of Zw1615+35 was not feasible due to the presence of 2 X-ray bright sources in the field.

From the ASCA observations of the Centaurus cluster, we selected the longest observation of the cluster center done in 1-CCD mode to analyze the emission within central 7'. Other observations are used to analyze the cluster emission in the 7'–30' radius region. We also excluded the Eastern part of the cluster which may have an infalling subgroup (Churazov et al. 1999).

We correct for the lower ASCA SIS normalizations relative to ASCA GIS following Iwasawa, Fabian & Nandra (1999). This increases our gas mass estimates by approximately 10%.

## 3. TEMPERATURE PROFILES

We present the derived temperature distributions using single-temperature fits in Fig.1 and the temperature profiles of the hotter component in the two-temperature fits in Fig.2. In the central spatial bins of the clusters exhibiting a presence of a colder temperature component, we also attempt the two-temperature fits. The single temperature fits are used to calculate  $kT_{unc}$  in Tab.1, while temperature of the hot component in the two-temperature fits is used to calculate  $kT_e$ . One can see from the Table that there is no difference for A400, A194 (however for this cluster the center is excluded anyway), A539, AWM4, and A2634, while changes in the weighted temperature for other cluster appear not to be very significant. In the single-temperature fits, the temperature appears to drop significantly with radius in A400, A2634, HCG94, in the outskirts of MKW3S, and also marginally in Cen. Adding a second temperature in the fits adds A2063 and marginally MKW4S to the list of clusters with declining temperature profiles. More evident is the removal of rising temperature profiles in A262, 2A0335+096, A2052, A779, Cen and marginally in MKW3S. The hot component is rather faint in the center and as was shown in case of M87 may be a spatially distinct from cold component (Finoguenov & Jones 2000). However, the use of a two-temperature model mimics the cooling-flow model of Johnstone et al. (1992, cf Buote 2000). To quantify the characteristics of the cold component, we present in Tab.2 the temperature, emissivity, and gas mass of this component. The corresponding cooling rates can then be derived from these values. It was pointed out by Fukazawa (1997), that the cold component of a two temperature fit in the range between 1 and 2 keV may reflect the potential of the central cD rather than being an indication of a cooling flow. While we cannot distinguish between these two possibilities with our present sample, in the

FDP sample our fits to A2029, A3112, and the A780 spectra resulted in temperatures for the cold components of  $\sim 5, 3$  and  $3$  keV, respectively. It is therefore more likely that these clusters have cooling flows.

TABLE 2  
CHARACTERISTICS OF THE CENTRAL COLD COMPONENT.<sup>b</sup>

Name	$kT_c$ keV	EM <sup>c</sup>	$M_{gas}$ $10^{11} M_{\odot}$
A262	1.259 (1.17:1.35)	2.747 (2.02:3.47)	0.545 (0.47:0.61)
MKW4S	1.437 (1.33:1.48)	0.147 (0.09:0.17)	0.504 (0.40:0.53)
MKW9	1.600 (1.49:1.71)	0.257 (0.21:0.28)	1.452 (1.31:1.51)
A2197	1.178 (1.04:1.30)	0.117 (0.03:0.23)	0.523 (0.29:0.74)
A4038	1.507 (1.31:1.73)	3.908 (2.22:5.60)	2.868 (2.16:3.43)
2A0335	1.533 (1.44:1.67)	6.602 (4.72:8.27)	5.508 (4.66:6.16)
HCG94	1.518 (0.79:2.05)	0.411 (0.12:0.67)	2.112 (1.12:2.71)
A2052	1.583 (1.44:1.70)	5.784 (4.25:7.59)	5.160 (4.43:5.92)
A779	1.017 (0.97:1.10)	0.211 (0.12:0.29)	0.347 (0.27:0.41)
MKW3S	1.898 (1.70:2.10)	3.934 (3.18:4.89)	7.980 (7.18:8.89)
CEN	1.622 (1.54:1.71)	15.05 (13.3:17.2)	1.213 (1.15:1.28)
A2063	1.521 (1.19:1.87)	0.075 (0.00:0.18)	0.617 (0.00:0.97)

<sup>b</sup> Errors are quoted on the 68% confidence level.

<sup>c</sup> The emission measures are quoted in units of  $10^{-17} \int n_e n_p dV / 4\pi D^2$ , i.e.  $10^{-3}$  times the XSPEC units for *norm*. Correction for SIS vs GIS normalizations of 1.2 has been made

Most of the clusters in our sample have temperature profiles similar to the universal temperature profile of Markevitch *et al.* (1998). Only 2A0335+096 can be considered as discrepant, similar to findings of Kikuchi *et al.* (1999). However, our conclusion regarding MKW3S favors the results of Markevitch *et al.* (1998). In MKW3S we detect a lower temperature in the outer annulus even with the single-temperature models. However, at the radius in question, the SIS data do not cover the Northeastern part of the cluster. The presence of high temperature gas in this region would account for our discrepancies with Kikuchi *et al.* (1999). Some of the clusters in this sample (A194, A539, AWM4, MKW9, A4038, A2052 and A779) suggest an isothermal temperature distribution. The implications of this result on the M-T relation are further discussed in Finoguenov, Reiprich & Boehringer (2001). Modeling of ASCA data is especially complicated in the presence of strong cooling flows (Markevitch 2000, private communication). Therefore, our observation of the apparent temperature declines in the non-cooling flow clusters A400 and A2634 is particularly important for confirmation of temperature gradients.

The steep rise in the central gas temperature we detect in the Centaurus cluster mimics the presence of the non-thermal component reported in Allen *et al.* (1999). Due to the limitations of the SIS data, i.e., the complex PSF and low sensitivity at high energies, a more detailed study must await XMM and Chandra observations.

Temperature and iron abundance profiles for the clusters reported in this paper were also analyzed by White (2000) using GIS data. A comparison of our temperature profiles with those in White shows remarkable agreement for single-temperature fitting (our Fig.1), while our results on the iron abundance supersedes in quality White (2000) results, because of the greater spectral resolution and sensitivity of the SIS compared to the GIS. For hotter clusters, the GIS iron abundance results have a similar quality with the SIS results of FDP. Given the differences in White's method for modeling of ASCA PSF effects (White & Buote 2000), this agreement reassures the robustness

of ASCA measurements.

#### 4. RADIAL DISTRIBUTION OF HEAVY ELEMENTS

##### 4.1. Iron

With a statistical threshold of 90%, an iron abundance gradient is observed in A400, A262, MKW4S, 2A0335+096, HCG94, MKW3S and Cen. Among these clusters, an Fe gradient outside the central 100 kpc is seen in A400, 2A0335+096, and Cen. A comparison with other ASCA measurements produces good agreement, except possibly for AWM4, where the presence of a strong point source complicates the analysis. The analytical fit of the Fe abundance in Cen from Ikebe *et al.* (1999) appears to be slightly more centrally concentrated. However, one should take into account the spatial width of our bins. We ascribe the abundance values to the center of the spatial bin, but the abundance values in each bin are dominated by the emission closer to the cluster center, which can explain our broader Fe distribution. Overall, good agreement between our results and Ikebe *et al.* (1999) serves as an argument against the suggestion of Buote (2000) about the underestimation of elemental abundances in the center of clusters due to 'overregularization'.

##### 4.2. Silicon, Neon and Sulfur

With a statistical threshold of 90%, Si abundance gradients are observed in A400, A262, and Cen. Only in A400 is there a significant decrease in the Si abundance beyond the central 100 kpc. A comparison with the results of Fukazawa *et al.* (1998) shows very good agreement, except possibly for AWM4 (our value is  $2\sigma$  higher).

No Ne abundance gradients are detected in this sample. Ne abundance are only significantly constrained in A262, MKW4S, MKW3S and Cen. A sulfur abundance gradient is detected in Cen excluding the central 100 kpc from consideration. The S/Fe ratio changes by much less than the Si/Fe ratio with radius, which was also noted by Fukazawa (1997). Central enhancements of Sulfur are marginally seen in 2A0335+096 and MKW4S and S abundance is constrained at any radius in A2197E, A400, A262, MKW9, A4038 and A2052.

#### 5. HEAVY ELEMENTS AT SIMILAR OVERDENSITY.

The derived elemental abundances in our sample of groups and clusters of galaxies span the range from 1/10 to a few times solar, even within a single system (*e.g.* Cen cluster). To compare the results between different systems, we need to choose an appropriate physical scale. The natural physical scale of a cluster is its virial radius and we thus compare data at given fractions of  $r_{180}$ . This is equivalent to comparing data at similar overdensity.

It is worth noting that the overdensity does appear to be a fundamental parameter for the metal enrichment, as indicated by the simulations of Cen and Ostriker (1999). Furthermore, the cluster morphological content, another potentially important factor for chemical enrichment, should be the same at the radius of comparison, since it depends on the local galaxy density (Dressler 1980).

In Tab.1 we show  $r_{180}$  for all the systems in our sample. Comparisons between systems are made at 1/5 and 2/5 of  $r_{180}$  (corresponding to overdensities of 8600 and 1600). We choose an outer radius of  $0.4r_{180}$  due to the limited extent of our observations. The inner radius of 1/5  $r_{180}$  is chosen to avoid the central

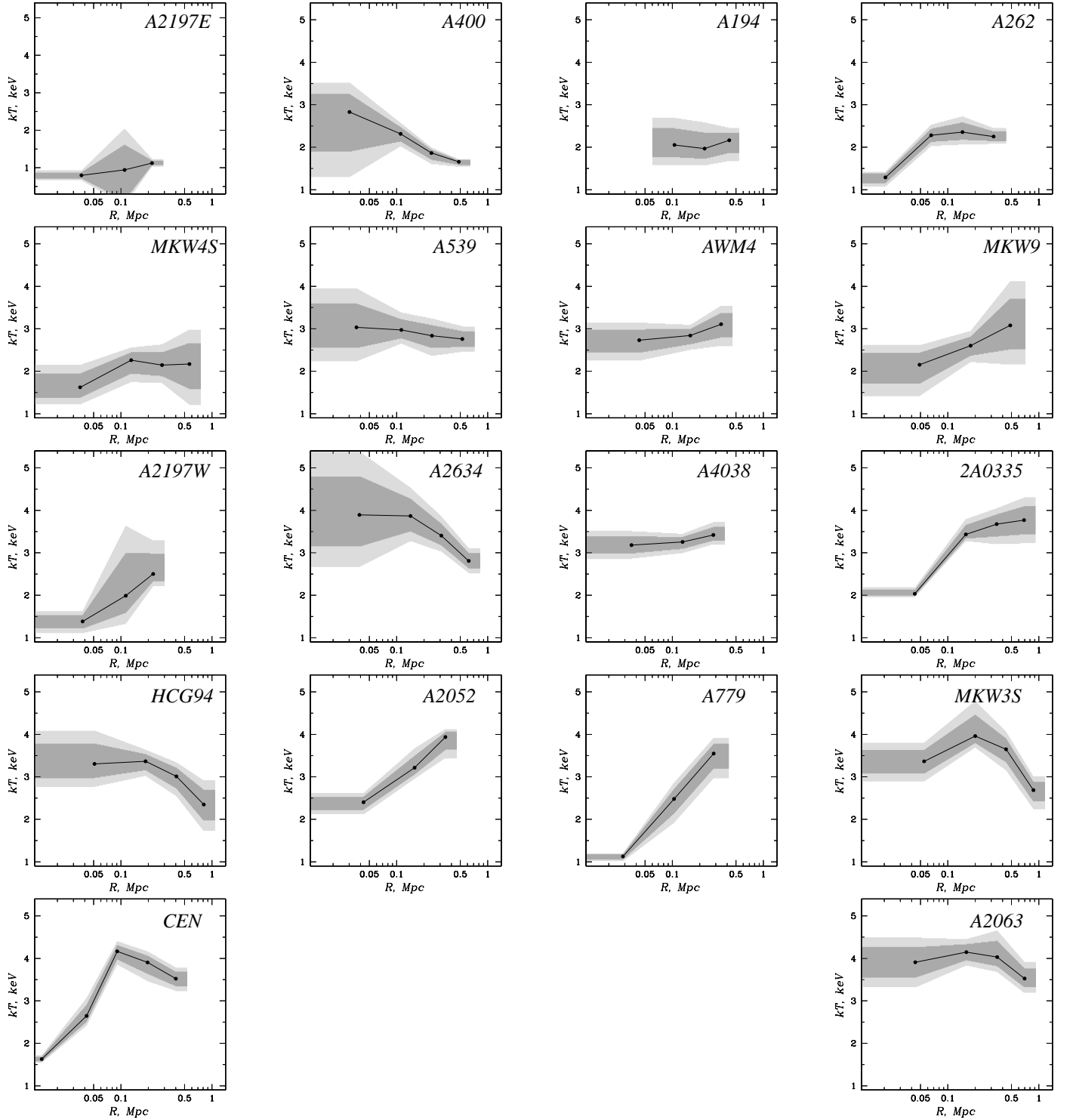


FIG. 1.— Temperature profiles, derived using a simple one-temperature model to fit the data. The solid lines correspond to the best-fit with filled circles indicating the spatial binning used in the analysis. Dark and light shaded zones around the best fit curves denote the 68 and 90 per cent confidence areas.

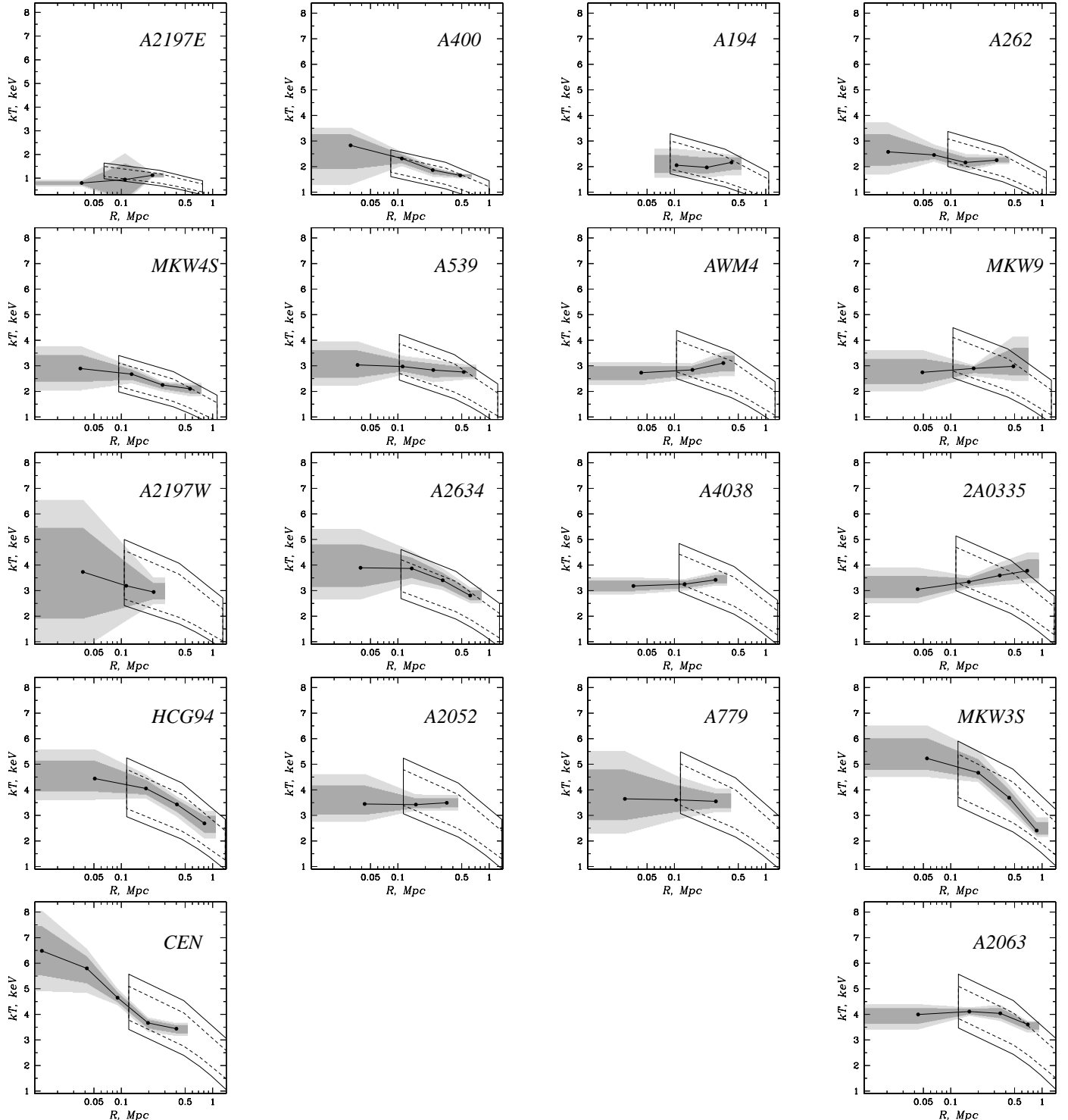


FIG. 2.— Corrected temperature profiles, derived considering a two-phase model for the center to fit the data. The solid lines correspond to the best-fit with filled circles indicating the spatial binning used in the analysis. Dark and light shaded zones around the best fit curves denote the 68 and 90 per cent confidence areas. Contours denote the range of temperatures found in Markevitch et al. (1998), scaled according to the luminosity weighted temperature of the cluster,  $kT_e$  (col. 14 in Tab.1) using virial units for radii (col. 16 in Tab.1).

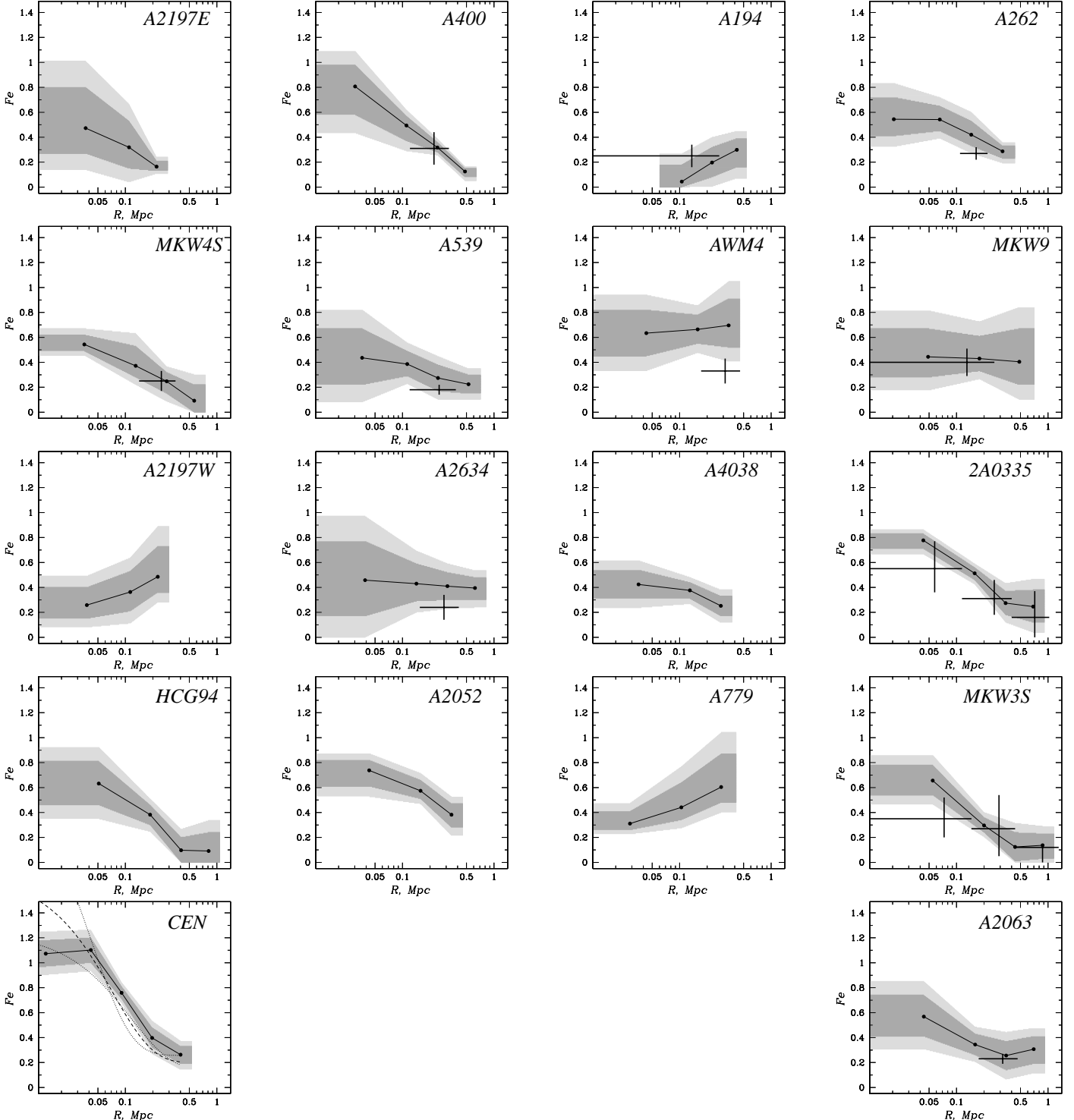


FIG. 3.— Derived Fe abundances (in units of  $4.68 \cdot 10^{-5}$  for iron number abundances relative to H). The solid lines correspond to the best-fit Fe abundances derived from the ASCA data. The filled circles indicate the spatial binning used in the analysis. Dark and light shaded zones around the best fit curves denote the 68 and 90 per cent confidence areas. Crosses on A400, A194, A262, MKW4S, A539, AWM4, MKW9, A2634 and A2063 panels show the results from Fukazawa et al. (1998) with radii of measurement from Fukazawa (private communication). Crosses on the 2A0335 and MKW3S plots denote the results of modeling of GIS data from Kikuchi et al. (1999) and similarly lines on Cen plot from Ikebe et al. (1999).

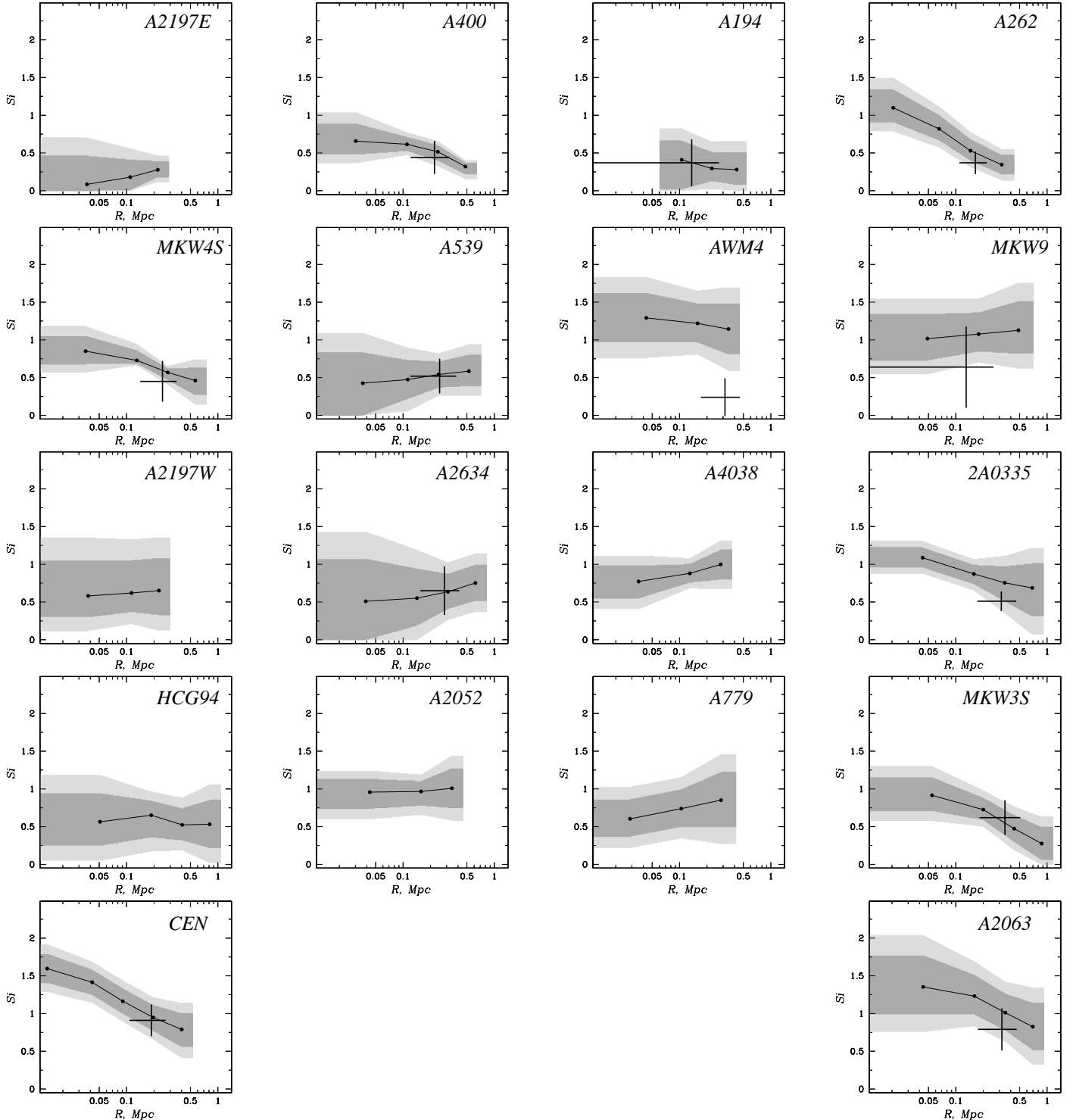


FIG. 4.— Derived Si abundances. The solid lines correspond to the best-fit Si abundances derived from the ASCA data. The filled circles indicate the spatial binning used in the analysis. Dark and light shaded zones around the best fit curves denote the 68 and 90 per cent confidence areas. Crosses on A400, A194, A262, MKW4S, A539, AWM4, MKW9, A2634, Cen and A2063 panels show the results from Fukazawa et al. (1998) with radii of measurement from Fukazawa (private communication).

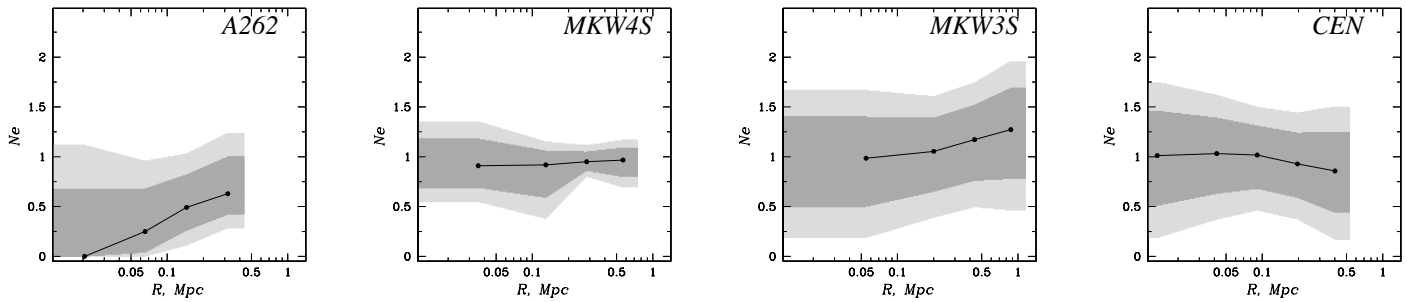


FIG. 5.— Derived Ne abundances. The solid lines correspond to the best-fit Ne abundances derived from the ASCA data. The filled circles indicate the spatial binning used in the analysis. Dark and light shaded zones around the best fit curves denote the 68 and 90 per cent confidence areas.

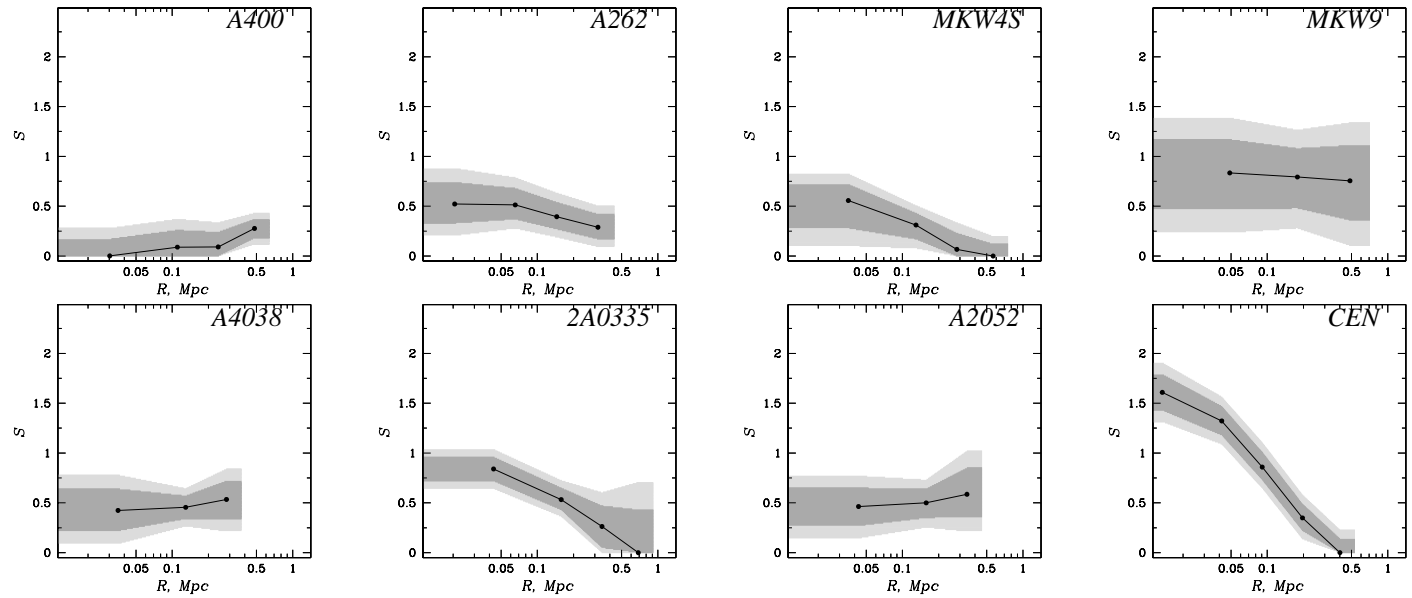


FIG. 6.— Derived S abundances. The solid lines correspond to the best-fit S abundances derived from the ASCA data. The filled circles indicate the spatial binning used in the analysis. Dark and light shaded zones around the best fit curves denote the 68 and 90 per cent confidence areas.

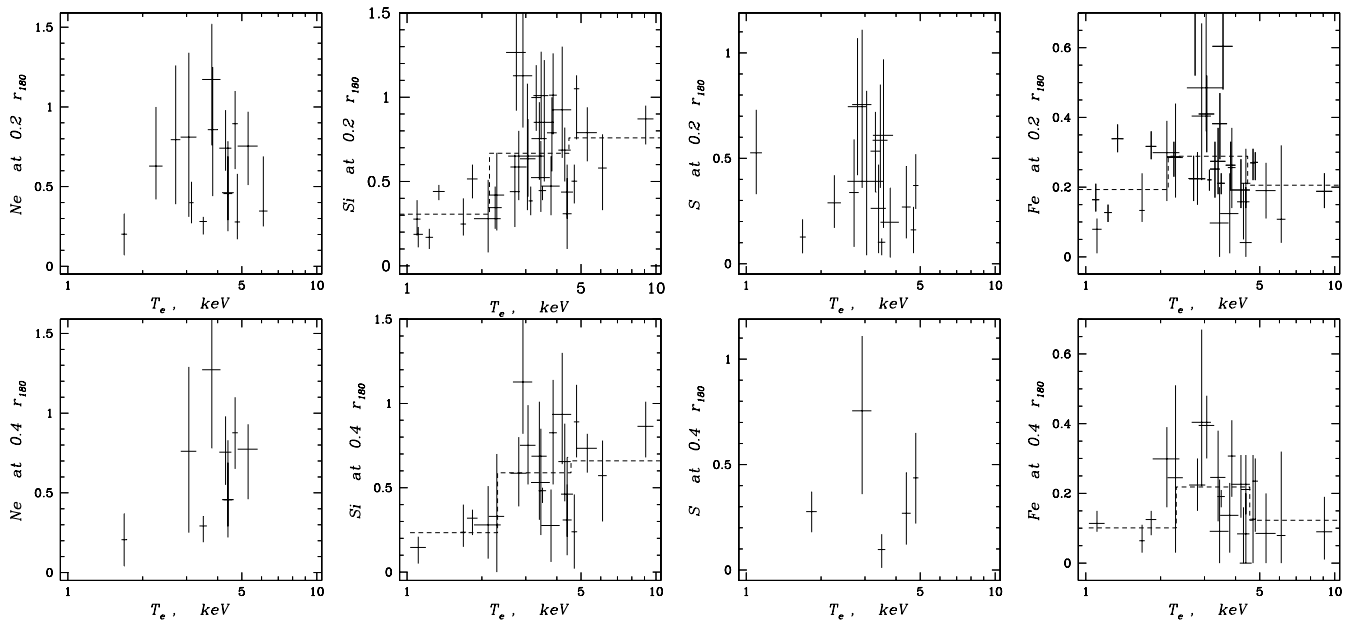


FIG. 7.— Ne, Si, S and Fe abundance determined at a given (0.2 and 0.4) fraction of the virial radius. Dashed lines in the Si and Fe figures denote the change of the averaged value.

200 kpc. Among the elements presented in Fig. 7, Ne and S do not reveal any distinct trend, due to large measurement errors.

A major difference between our work and some earlier results (e.g. Renzini et al. 1993) is the dependence of the Fe abundance on gas temperature at lower temperatures. We do not find an increase in the Fe abundance near 1 keV as previously reported. Instead, the Fe abundances at  $0.2r_{180}$  are similar among groups and clusters with a tendency for the Fe abundance to decrease at lower overdensities (compare the values at  $0.2r_{180}$  and  $0.4r_{180}$ ). The average trends in the Fe abundance at  $0.2r_{180}$  with temperature plotted in Fig. 7, are in good agreement with the findings of Fukazawa et al. (1998). There is a peak in the Fe abundance of 0.3 solar for cool clusters, with hotter clusters having average iron abundances of 0.2 solar.

In contrast, the Si abundances increase strongly with gas temperature, starting from 1/5 solar in groups and reaching solar values in hot clusters. This agrees with the previous findings of Fukazawa et al. (1998). This drastic difference between the Si and Fe abundances reflects the level of SN II retainment indicated by the Si abundance, while the nearly constant Fe abundance reflects the equal role of SN Ia in groups and clusters of galaxies (e.g. FDP). To determine the relative enrichment from different supernovae types, we adopt the yields in FDP, given by,  $y_{Si} = 0.133M_{\odot}$ ,  $y_{Fe} = 0.07M_{\odot}$  for SN II yields and  $y_{Si} = 0.158M_{\odot}$ ,  $y_{Fe} = 0.744M_{\odot}$  for SN Ia.

In Fig. 8 we show the Fe and Si mass accumulated within 1/5 and 2/5 of the  $r_{180}$  expressed in a form useful for the study of element production, i.e., the  $M/L_B$  ratio ( $h_{50}^{-1/2}M_{\odot}/L_{\odot}$ ). The light and gas within the central 200 kpc are not included in this calculation for systems with cD galaxies. In Fig. 8 we also show the IMLR for each SN type. As can be seen in Fig. 8, both the Si M/L and the SN II Fe M/L increase by a factor of 10 between groups and clusters of galaxies. In contrast, the difference in Fe M/L and SN Ia Fe M/L is less prominent, especially at  $0.4r_{180}$ . For comparison, we also plot in Fig. 8 the corresponding gas mass fractions. Between 0.2 and 0.4  $r_{180}$  there is a significant change in  $f_{gas}$ , with clusters tending to have similar gaseous fractions at large radii. These results can be compared with the low scatter in gas fractions found at smaller overdensities by Ettori & Fabian (1999) and Vikhlinin et al. (1999).

### 5.1. SN II and the Preferential Infall Scenario

The main goal of this section is to explain the different observed Si abundances in these systems. In particular, we are interested in the dependence of the Si abundance on the gas retainment (or accretion) in these systems. To illustrate this idea, consider an outflow of material from a group, caused by some form of heating. Such a scenario can explain the reduced gas fractions and mass in elements inside groups, but such a scenario cannot change the Si abundance.

In FDP, we proposed that the absence of strong gradients in alpha-elements implies that SN II enrichment occurred prior to cluster collapse. We also note that the Si abundance does not vary significantly between  $0.2r_{180}$  and  $0.4r_{180}$  (see Figs. 7 and 8) even though there is a significant change in  $f_{gas}$  between these radii. This result also requires that the enrichment of the ICM with Si occur before the gas distribution in these systems has been established. Thus, we propose a *preferential infall scenario* to explain the different levels of alpha-elements in these systems. In this scenario, intergalactic gas, after being enriched with SN II ejecta, becomes too hot (or has too high an entropy) to accrete into the shallow potential wells of cold systems, so

only the low-entropy metal-poor gas is accreted onto groups. The more strongly enriched, higher-entropy gas can only be accreted onto rich clusters.

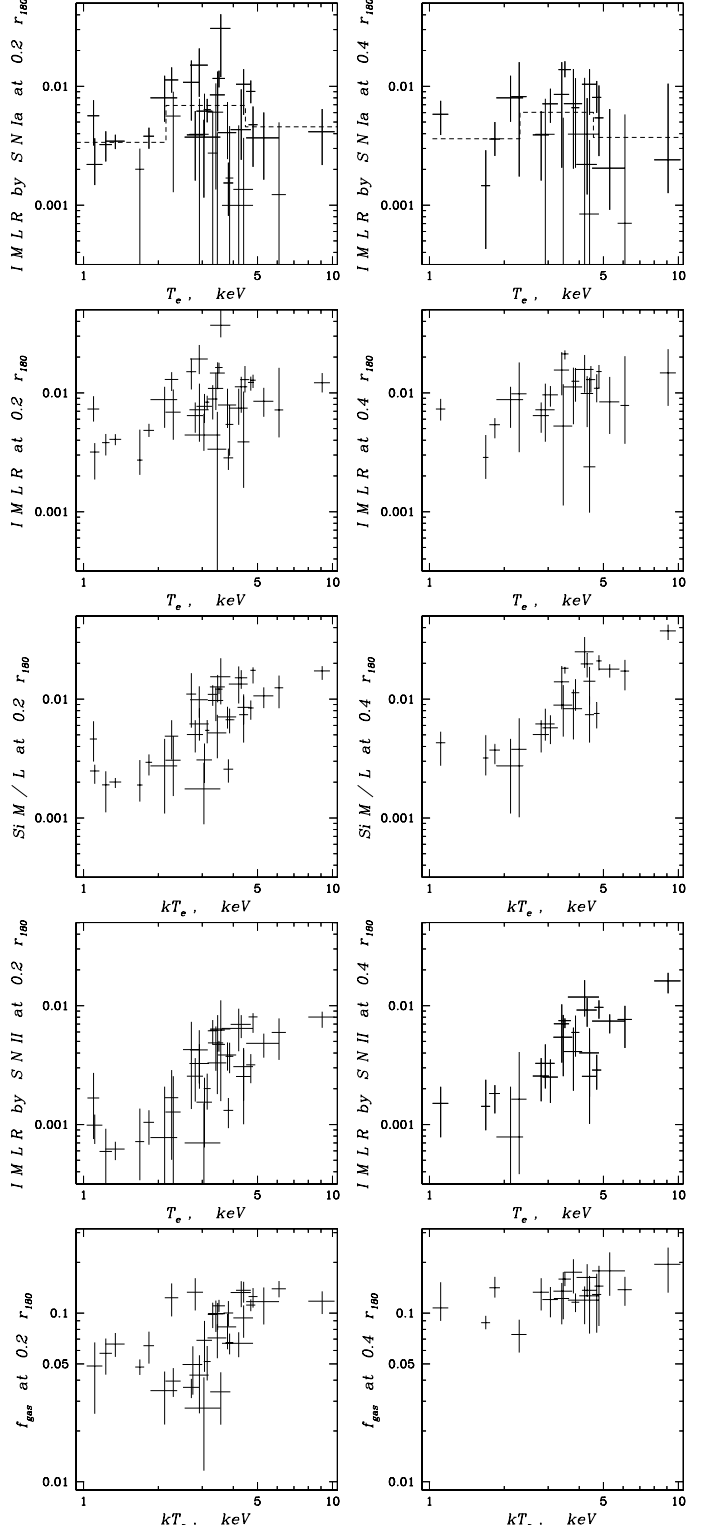


FIG. 8.—  $M/L_B$  ratios for Fe, Si and SN type II and Ia contribution to Fe  $M/L_B$ . Behavior of gaseous fraction is shown at the bottom. Values are displayed at 0.2 and 0.4  $r_{180}$ . Dashed lines in the SN Ia figures denote the change of the averaged value.

In order for this scenario to work, the excess entropy of the SN-preheated gas should exceed the entropy increase produced during the accretion and shock heating of the gas in groups.

It is worth noting that the entropy increase due to shocks and the entropy increase due to preheating exhibit different scaling relations depending on the cluster formation redshift, *e.g.* Ponman, Cannon, Navarro (1999). This provides a possible test of the above scenario, through future observations of the Si abundance levels in a large sample of groups. A large scatter in formation epochs for groups, as suggested by simulations, may be a reflection of the relative importance of preheating vs accretion shock heating, and may allow a more precise determination of the actual energy released by SNe II in the form of preheating.

Since between the 0.2 and 0.4  $r_{180}$  Si abundance is constant, as well as  $M_{tot}/L_B$  ratio, the observed differences in SN II Fe M/L ratio at the 0.2 and 0.4  $r_{180}$  simply follow the changes in  $f_{gas}$ .

One possible explanations for the reduced gas fractions in cold clusters is that the baryons are contained in the form of stars and the baryon fraction is actually a constant. However, such a scenario cannot reproduce the observed behavior in the Si abundance, since the consumption of any gas will change the mass of elements in the ICM, but will not alter the abundances.

In the scenario presented above, we propose that the trend in the observed Si abundance is produced by varying degrees of SN II retainment. In the following, we discuss an alternative 'closed-box' scenario, in which the increase in the Si abundance with gas temperature results from a dependence of the star formation on the gravitational potential of the system. This requires that SN II are more common in hotter clusters, either because their galaxies are more massive (Diaferio 1999) and more metals per given light are released into the ICM, or the IMF is *top-heavy* in the host galaxies of hotter clusters (Larson 1998). In such a case, SN II are favored in massive systems, resulting in higher [Si/H] and Si M/L ratios. In terms of the slope of the IMF, the observed Si abundances require an IMF slightly steeper than the Scalo IMF for systems cooler than 3 keV, and an IMF that is slightly more top-heavy than a Salpeter IMF in hot clusters (using the calculations of the SN II contribution to the IMLR from Renzini et al. 1993, who adopt  $y_{fe}$  from SN II consistent with our definition;  $IMLR(x=1.7)=0.003 \Rightarrow IMLR(x=1.35)=0.009 \Rightarrow IMLR(x=0.9)=0.035$ .) We note that only the measurement for A2029 at 2/5  $r_{180}$  exceeds the amount of IMLR predicted for a Salpeter IMF.

## 5.2. SN energy input and the scaling relations.

Preheating of the intergalactic medium by supernovae has long been considered a possible explanation for the observed deviation of cluster scaling laws from theoretical expectations based on simple gravitational collapse. More recently, the amount of preheating was estimated to be 1–3 keV per particle in order to explain the entropy floor in cool systems (Ponman et al. 1999; Loewenstein 2000; Wu et al. 1999). This amount of energy has been considered too high to be produced by SNe heating alone and heating by AGNs has been suggested as an alternative solution to the problem (Wu et al. 1999).

Our observations provide for the possibility of determining the amount of energy associated with SNe in a robust way using the measured Si abundances. The advantage of this method consists in the similar Si yields for different SNe types, so a separation between SN Ia and SN II is not required to calculate the energy released.

In Fig.9 we show our estimate for the energy associated with SN feedback, assuming that each SN provides  $0.14M_{\odot}$  of Si ( $y_{Si}$ ) and releases  $E_{SN} = 10^{51}$  ergs of mechanical energy. Based on these assumptions a solar abundance of Si ( $A_{Si}$ ) corresponds

to 1.6 keV/particle ( $E_{SN}A_{Si}\mu m_p/y_{Si}$ , where  $\mu = 0.6$ ,  $m_p$  – proton mass). As can be seen from Fig.9, the data show a flattening in the SN energy input around the cluster temperature of 3 keV. This means that for systems hotter than 3 keV, SN ejecta makes little difference on the gas thermodynamics and that these systems should be self-similar. In fact, this is exactly what is observed (Ponman et al. 1999). If AGNs were responsible for preheating the gas in clusters, this trend with the Si abundance would not be reproduced.

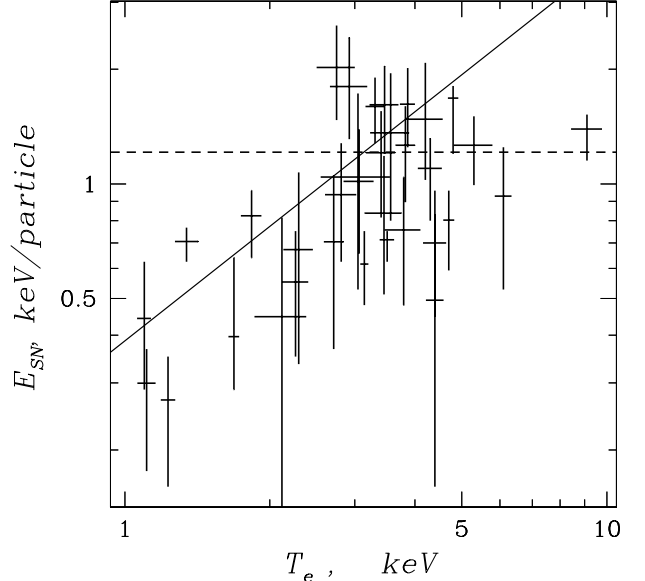


FIG. 9.— Thermal energy supplied by both types of SNe associated with measured Si abundance. Under assumption that each SN provides  $0.14M_{\odot}$  of Si and releases  $10^{51}$  ergs in a form of thermal energy, a solar abundance of Si correspond to energy release of 1.6 keV per particle. The data is flat above 3 keV temperature with mean SN energy of 1.2 keV per particle.

There exists a significant discrepancy in the normalizations of the  $M-T$  relation between simulations (*e.g.* Evrard et al. 1996) and observations (Horner et al. 1999). One possible explanation is that the observed X-ray temperatures are  $\sim 40\%$  higher compared to that expected from pure gravitational heating. The solid line in the figure shows the SN feedback needed to reconcile the normalizations of the  $M-T$  relations. As can be seen from the figure, this fit matches our measurements below 3 keV. However, for a similar SN-heating scenario to hold for a 10 keV cluster, the observed Si abundance should reach 2 times solar, which is not observed (Fukazawa et al. 1998). As a result, mass estimates for clusters hotter than  $\sim 6$  keV are expected to get progressively closer to simulations of Evrard et al. (1996), as  $\frac{\Delta T}{T}$  decreases with T. Application of this scenario to the observed  $M-T$  relation is further discussed in Finoguenov, Reiprich, Boehringer (2001).

We note that the preferential infall scenario naturally supports the two levels of entropy ( $250 \pm 100$  and  $500 \pm 200$  keV  $\text{cm}^2$ ), that are introduced in Tozzi & Norman (2001) to explain the  $L-T$  relation. It is remarkable that at  $0.4r_{180}$  the observed entropy in groups begins to exceed the adopted preheating level, there is no drastic difference in the gas fraction among these systems (see Fig.8). Yet, the Si abundance does not increase in groups, which implies that there is no substantial enrichment at later times and that previously enriched gas escaped the group's surroundings. This escaped gas can enrich a cluster of galaxies sitting on the same filament and create enhanced Si abundance. Fukugita et al. (1998) estimated the total amount of baryons in groups maybe similar to that in clusters. Therefore, hot clus-

ters may accrete a substantial amount of alpha elements (up to 50%), but not (yet?) the galaxies.

The largest uncertainty in estimating the mechanical heating from SNe comes from radiative losses. Under the assumption of a thermal wind, where the wind velocity is equal to the escape velocity of a galaxy, Renzini (2000) obtained a value for SN energy input that is 10% of the initial energy released. We argue, that this is a lower limit on SN heating. Wind velocities up to a  $\sim 1000$  km/sec implied by the assumption of low radiative losses are justified in Lloyd-Davies et al. (2000). If metals are ejected via thermal winds, as assumed by Renzini (2000), then most of the metals will remain bound to groups. The observed entropy at  $(0.2r_{180})$  in groups is approximately  $300$  keV cm $^2$ . At the corresponding formation epoch the pre-heated gas entropy is  $500\Delta E$  keV cm $^2$  (following Lloyd-Davies et al. 2000), where  $\Delta E$  is in keV per particle. If the assumption of thermal winds is correct, the preheating entropy is then only  $50$  keV cm $^2$ , which cannot produce a significant loss of enriched gas from group potentials. Also, no infall avoidance of enriched gas is seen in hotter systems, where the entropy exceeds  $700$  keV cm $^2$ , leaving little room for alternatives. Therefore, we conclude that our estimate of the energy input from SNe is justified. One important detail in calculating the energy released by SNe is that we only detect in clusters of galaxies the elements that successfully escaped from the galaxies (which gives a rough estimate of  $f_{ej}$  of 2/3 for modeling of the starbursts, just from observing two thirds of metals in ICM). Some of the material that experiences large radiative losses will inevitably remain bound to the galaxy (e.g. Larson & Dinerstein 1975).

### 5.3. SN Ia products as an indicator of the cluster formation age.

The retainment of SN Ia products shown in Fig.8 reveals a significant differences between systems. On average, cool clusters ( $T = 2-4$  keV) have an SN Ia IMLR that is 1.5 times higher compared to hot clusters. In explaining the observed variations in the SN II products in the ICM, we speculated on the preferential accretion of low-entropy low-abundance gas. Differences in the SN Ia products cannot be explained in this way. In fact, as we noted above, clusters that are rich in SN Ia products are not necessarily the hottest ones. Furthermore, the lower Fe abundance at higher gas mass fraction suggests that Fe enrichment occur mostly after the gas density distribution was established, and not before cluster collapse. In this section we discuss possible mechanisms that may lead to variations in the amount of SNe Ia ejecta in the ICM.

In the classical scenario for the formation of elliptical galaxies, most of the stars form in a short burst of star formation at early times. SN Ia (long lived secondary star) will continue to explode and the SN Ia products will not be recycled because of the lack of star formation, but will continuously build up over the lifetime of the galaxy. Thus, in a given galaxy, the SN Ia products will remain in the ISM and their abundance will increase with time, until the host galaxies fall into the dense ICM environment. If striping is continuous after the galaxy has entered the cluster the SN Ia Fe M/L will be constant. Since this is not observed, we need to modify this standard scenario.

Possible assumptions are

- The galaxy recycles its elements through star formation while outside the cluster (may be due to ellipticals being not the only source of SN Ia products in clusters of

galaxies)

- The halos of infalling groups/galaxies are stripped at very large distances

Both scenarios can be characterized as attempts to hide the SN Ia products before the galaxy's infall, either in the stellar population of the host galaxies, or by spreading them through the outskirts of clusters. There are certain observational and theoretical grounds for the above modifications. First, it is found in studies of star formation in galaxies, that galaxies probably significantly reduce their star formation after falling into clusters (Balogh et al. 1998; Poggianti et al. 1999). Second, in hydrodynamical simulations (Klypin, private communication), the gaseous content of infalling groups of galaxies is segregated (stripped) from the infalling galaxies at the outskirts of clusters. Third, observed galaxies entering clusters (e.g. M86) show that the amount of metals associated with their halos is  $\sim 10^{-4}$  in terms of Fe M/L ratio, which is only a few percent of the ICM value.

What are the observational consequences of the proposed modifications? Only SN Ia explosions occurring after galaxies infall will contribute to the SN Ia ICM enrichment. First of all, if clusters form from inside out by the gradually accretion of galaxies (e.g. Klypin et al. 1999), then one expects that the central parts of clusters should be exposed to SN Ia enrichment for the longest time. This scenario reproduces the Fe M/L ratio gradient discussed in FDP. The rising Fe M/L ratios detected in compact groups (FDP) can be understood within the context of this scenario if the galaxies have collapsed only recently onto the center of groups (in agreement with a statement that compact groups are dynamically young). Second, the Fe M/L ratio should be correlated with the formation of the galactic components of clusters, since clusters that form earlier will retain more ejecta. Within this scenario, we can easily explain the scatter in the Fe M/L as well as the peak in Fe M/L for cold clusters in view of direct similarity to Butcher-Oemler effect (e.g. Kauffmann 1995). We can therefore test our scenario by comparing with simulations of large-scale structure.

To derive the redshift of cluster formation from the observed mass of heavy elements, we have to assume a present-day SN Ia rate and the redshift dependence of the SN Ia rate. Soon (with the advent of the NGST) this will be a nicely determined function, at present, in addition to the local measurements (Cappellaro et al. 1997) there is only one point at  $z = 0.4$  from SN Ia Cosmology Project (Pain et al. 1996) obtained for field galaxies. Following a suggestion of Renzini et al. (1993), we assume a power law dependence of SN Ia rate with time, using the two measured points. We adopt for this calculation  $h = 0.75$  (and rescale our IMLRs), local  $R_{SNIA} = 0.2$  SNu (1 SN per century per  $10^{10}L_{B\odot}$ ); adopting this value we consider all the galaxies as SN Ia producers),  $s = 2$  (see Eq.7 in Renzini et al. 1993). The use of  $s = 2$  (which implies a greater SN Ia rate in the past) is also justified by the large amount of Fe attributed to SN Ia in our measurements. For example, a time-independent rate of SN Ia can only provide about  $\sim 10\%$  of the measured value (this consideration is similar to the estimate of Renzini et al. 1993). We also consider two different cosmologies:  $\Omega = 1$  and  $\Lambda$ CDM with  $\Omega_m = 0.3$ .

The calculation itself could be expressed as

$$M_{Fe,SNIA} = \int_{t(z=0)}^{t(z=\infty)} L_{z=0} \theta(t - t_{formation}) A(t) dt$$

where  $A(t)$  is the SN Ia metal production rate per unit luminosity. We approximate the evolution of the galactic components of clusters by  $L_{z=0}\theta(t - t_{formation})$ , *i.e.* by observing the present-day light for some period of time ( $\theta$  is equal to 1 after cluster collapse epoch and 0 before). The results of this calculation are shown in Fig.10. We choose a redshift binning of 0.5 to improve the statistical significance of the points and yet retain the most useful information. Every cluster is added as a Gaussian of width corresponding to the uncertainty of the measurement. In order for these plots to be directly compared with observations, we should correct for the incompleteness of our sample. To accomplish this we used the cluster number function from Henry & Arnaud (1991), counting systems colder than 2 keV as 2 keV clusters.

In the plot we also show the analytical and numerical results on the formation of clusters (Lacey & Cole 1993), following the formulae presented in Balogh et al. (1999) for  $\Omega_m = 0.3$ . We set the mass fraction of clusters whose formation we want to trace to 40%, representing the ratio of the mass at 1/5 of virial radius (chosen for comparison with the SN Ia products) to the total virialized mass of the cluster and do the calculation for two masses ( $2$  and  $5 \times 10^{14} M_\odot$ ), characterizing two subsamples, shown in Fig.10. In making comparisons with the simulations, we implicitly assume that there is no segregation between the clustering of mass and light. As can be seen from the figure, formation of the central 40% of the mass in the nearby clusters is shifted to earlier epochs.

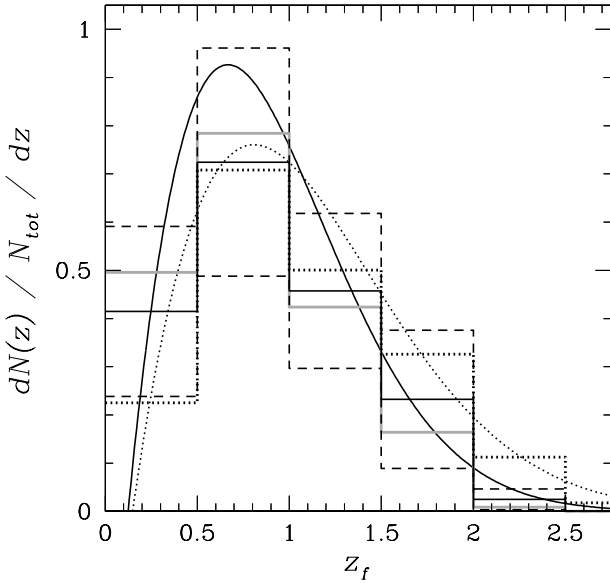


FIG. 10.— Redshifts of cluster formation deduced from Fe M/L ratio attributed to SN Ia. We correct for incompleteness of our sample using number function of Henry & Arnaud (1991). Black solid histogram shows calculation for the bright end of the sample ( $kT > 4$  keV), calculated for  $\Lambda$ CDM, with dashed histograms indicate the number count errors at 68% confidence level. Grey histogram shows calculation for  $\Omega = 1$ . Dotted histogram shows the calculation for the whole sample, assuming  $\Lambda$ CDM. Predictions from numerical simulations of structure formation (Lacey & Cole 1993), calculated using the formulae in Balogh (1999) for  $\Omega_M = 0.3$ , are shown for formation of first 40% of  $M = 5 \times 10^{14} M_\odot$  (solid line) and  $M = 2 \times 10^{14} M_\odot$  (dotted line), corresponding to the averaged mass of two samples shown.

The remarkable similarity between the distribution of formation redshifts derived here with the calculations of Lacey & Cole (1993) lends support to our explanation for the observed scatter in SN Ia Fe M/L ratio being due to differences in the

epoch of cluster formation. The exact meaning of Fig.10 is the formation of a certain part of the studied clusters ( $0.2r_{180}$ ). Similar plots can be done for any overdensity and can thus provide an effective mechanism for tracing the formation of large-scale structure.

## 6. CONCLUSIONS

By combining a new analysis of 18 cool clusters with our previous work we have a sample of clusters that span a factor of 10 in temperature. We derive the following conclusions based on abundance measurements at  $0.2r_{180}$  and  $0.4r_{180}$ .

- Groups and cool clusters preferentially accreted low-entropy low-abundance gas as best illustrated by the strong correlation between Si abundance and emission-weighted gas temperature of clusters. This supports the claim that energetic SNe II winds, driven at earlier epochs by star-burst galaxies, are responsible for preheating the gas.
- We detect a drastic change in the behavior of the gas mass fractions between  $0.2r_{180}$  and  $0.4r_{180}$  which are not accompanied by changes in the Si abundance. This requires that the enrichment by Si (SN II) occurs before the observed gas distribution was formed. Lower Fe abundances at higher gas mass fractions suggests that the SN Ia enrichment also occurred after gas density distribution was established. Accounting for the baryons in stars cannot solve the problem of the low gas mass fractions in low-mass systems.
- The energy per particle associated with SN explosions, when plotted against the emission-weighted system temperature, exhibits a break at 3 keV. At comparable temperatures many cluster scaling relation start to deviate from self-similarity (*e.g.* Ponman et al. 1999). This proves the importance of SN feedback on the formation of the gaseous component of clusters.
- We observe a significant scatter in the amount of SN Ia products between systems, with cool clusters among the most SN Ia rich systems. We propose an explanation based on the distribution of cluster formation redshifts. A comparison of the predicted distribution of formation redshifts of our sample with analytical formulation by Lacey & Cole (1993) for  $\Omega_m = 0.3$  demonstrates good agreement.

## ACKNOWLEDGMENTS

MA thanks S. Maurogordato for fruitful discussions on cluster photometry and for providing her background subtraction code. MA thanks E. Vangioni-Flam and M. Cassé for fruitful discussion. AF acknowledges useful discussions with S. Borgani, S. Gottloeber, A. Klypin, C. Metzler, J. Muecket, V. Mueller and P. Tozzi. Authors thank the referee for useful comments on the manuscript. AF acknowledges support from Alexander von Humboldt Stiftung during preparation of this work. The authors acknowledge the devoted work of the ASCA operation and calibration teams, without which this paper would not be possible. This work was partially supported by NASA grant NAG5-3064.

## REFERENCES

Allen S.W., Fabian A.C., Johnstone R.M., Arnaud K.A., Nulsen P.E.J., 1999, MNRAS, subm., (astro-ph/9910188)

Anders E. and Grevesse N. 1989, *Geochimica et Cosmochimica Acta*, 53, 197

Arnaud M., Rothenflug R., Boulade O., Vigroux L. and Vangioni-Flam, 1992, A&A, 254, 49

Arnouts S., de Lapparent V., Mathez G., Mazure A., Mellier Y., Bertin E., Kruszewski A., 1997, A&AS, 124, 163

Cappellaro E., Turatto M., Tsvetkov D., Bartunov O., Pollas C., Evans R. and Hamuy M. 1997, A&A, 322, 431

Balogh M.L., Schade D., Morris S., Yee H., Carlberg R., Ellingson E. 1998, ApJ, 504, 75

Balogh M.L., Babul A., Patton D.R., 1999, MNRAS, 307, 463

Benítez N., Broadhurst T., Rosati P., Courbin F., Squires G., Ligman C., Magain P. 1999, ApJ, 527, 31

Buote D., 2000, MNRAS, 311, 176

Burke B.E., Mountain R.W., Harrison D.C., Bautz M.W., Doty J.P., Ricker G.R. and Daniels P.J., 1991, IEEE Trans., EED-38, 1069

Cen R., Ostriker J. P., 1999, ApJL, 519, L109

Churazov E., Gilfanov M., Forman W., Jones C., 1996, ApJ, 471, 673

Churazov E., Gilfanov M., Forman W., Jones C., 1999, ApJ, 520, 105

Cirimele G., Nesci R. and Trèvese D. 1997, ApJ, 475, 11

Cirimele G., Nesci R., Trèvese D., 1998, ApJ, 495, 509

D'Ercole A. and Brighenti F. 1999, MNRAS, 309, 941

Diaferio A., 1999, Proc. of Turku Meeting, (astro-ph/9908263)

Dixon, K., Godwin J., Peach J., 1989, MNRAS, 239, 459

Dressler, A., 1980, ApJ, 236, 351

Ettori S. and Fabian A. 1999, MNRAS, 305, 834

Evans A., Metzler C. and Navarro J. 1996, ApJ, 469, 494

Fabian A., Arnaud K., Bautz M., Tawara Y. 1994, ApJ, 436, 63

Finoguenov A., Jones C., Forman W. and David L., 1999, ApJ, 514, 844

Finoguenov A. and Ponman T.J., 1999, MNRAS, 305, 325

Finoguenov A. and Jones C., 2000, ApJ, 539, 603

Finoguenov A., David L. P., Ponman T. J., 2000, ApJ, 544, 188

Finoguenov A., Reiprich T., Boehringer H., 2001, A&A, 368, 749

Fukazawa Y., 1997, PhD Thesis, Uni. of Tokyo

Fukazawa Y., Makishima K., Tamura T., Ezawa H., Xu H. et al. 1998, PASJ, 50, 187

Fukugita M., Hogan C.J., Peebles P.J.E., 1998, ApJ, 503 518

Girardi M., Giuricin G., Mardirossian F., Mezzetti M. and Boschin W. 1998, ApJ, 505, 74

Green M., Godwin J., Peach, 1990, MNRAS, 243, 159

Henry J. P., Arnaud K. A. 1991, ApJ, 372, 410

Horner D., Mushotzky R., Scharf C. 1999, ApJ, 520, 78

Ikebe Y., Makishima K., Fukazawa Y., Tamura T., Xu H., Ohashi T., Matsushita K. 1999, ApJ, 525, 58

Iwasawa K., Fabian A., Nandra K. 1999, MNRAS, 307, 611

Jerjen H., Dressler A., 1997, A&A Suppl.Ser. 124, 1

Jerjen H., Tammann, 1997, A&A, 1997, 321, 713

Johnstone R.M., Fabian A.C., Edge A.C., Thomas P.A., 1992, MNRAS, 255, 431

Kauffmann G., 1995, MNRAS, 274, 153

Kikuchi K., Furusho T., Ezawa H., Yamasaki N., Ohashi T., Fukazawa Y., Ikebe Y., 1999, PASJ, 51, 301

Klypin A., Gottlöber S., Kravtsov A., Khokhlov A. 1999, ApJ, 516, 530

Lacey C., Cole S., 1993, MNRAS, 262, 627

Larson R. B. and Dinerstein H. L. 1975, PASP, 87, 911

Larson R. B., 1998, MNRAS, 301, 569

Liedahl D.A., Osterheld A.L. and Goldstein W.H. 1995, ApJ (Letters), 438, L115

Lloyd-Davis E.J., Ponman T.J., Cannon D.B., 2000, MNRAS, 315, 689

Loewenstein M., 2000, ApJ, 532, 17

Markevitch, M., Forman, W. R., Sarazin, C. L., & Vikhlinin, A. 1998, ApJ, 503, 77

Metzler C.A. & Evrard A.E. 1994, ApJ, 437, 564

Mewe R., Gronfelschild E.H.B.M. and Oord G.H.J. 1985, A&A (Supplement Series), 62, 197

Mewe R. & Kaastra J. 1995, *Internal SRON-Leiden report*

Mushotzky R.F., Loewenstein M., Arnaud K.A., Tamura T., Fukazawa Y., Matsushita K., Kikuchi K. and Hatsukade I. 1996, ApJ, 466, 686

Nikogossyan, E., Durret F., Gerbal D., Magnard, F. 1999, A&A 349, 97

Ostriker E., Huchra J.P., Geller M.J., Kurtz M., 1988, AJ, 96, 1775

Pain R., Hook I., Deustua S., Gabi S., Goldhaber G. et al. 1996, ApJ, 473, 356

Poggianti B., Smail I., Dressler A., Couch W., Barger A., Butcher H., Ellis R., Oemler A. 1999, ApJ, 518, 576

Ponman T.J., Cannon D.B., Navarro J.F. 1999, Nature, 397, 153

Press W.H., Teukolsky S.A., Vetterling W.T., Flannery B.P. 1992, Numerical recipes in FORTRAN

Renzini A., Ciotti L., D'Ercole A., Pellegrini S. 1993, ApJ, 419, 52

Renzini A., 2000, Proc. LSS Symp., Santorini, p.103, (astro-ph/0001312)

Sakai S., Giovanelli R., Wegner G., 1994, AJ 108, 33

Snowden S.L., McCammon D., Burrows D.N. and Mendenhall J.A. 1994, ApJ, 424, 714

Strickland D.K., Stevens I.R., 2000, MNRAS, 314, 511

Tanaka Y., Inoue H. and Holt S.S. 19L37, PASJ, 84,46

Tozzi P., Norman C., 2001, ApJ, 546, 63

Trèvese D., Cirimele G., Cenci A., Appodia B., Flin P., Hickson P., 1997, A&A Suppl.Ser., 125, 459

Trèvese D., Cirimele G., Appodia B. 1996, A&A, 315, 365

Truemper J. 1983, *Adv. Space Res.*, 2, 241

Vikhlinin A., Forman W., Jones C., 1999, ApJ, 525, 46

White D.A., 2000, MNRAS, 312, 663

White D.A., Buote D.A., 2000, MNRAS, 312, 649

Wu K., Fabian A., Nulsen P., 2000, MNRAS, 318, 889